General Disclaimer

One or more of the Following Statements may affect this Document

- This document has been reproduced from the best copy furnished by the organizational source. It is being released in the interest of making available as much information as possible.

- This document may contain data, which exceeds the sheet parameters. It was furnished in this condition by the organizational source and is the best copy available.

- This document may contain tone-on-tone or color graphs, charts and/or pictures, which have been reproduced in black and white.

- This document is paginated as submitted by the original source.

- Portions of this document are not fully legible due to the historical nature of some of the material. However, it is the best reproduction available from the original submission.

Produced by the NASA Center for Aerospace Information (CASI)

NASA Technical Memorandum 82850

(NASA-TM-82850) LARGE DISPLACEMENTS AND STABILITY ANALYSIS OF NONLINEAR PROPELLER STRUCTURES (NASA) 18 p HC A02/MF A01 CSCL 20K

N82-31707

Unclas
G3/39 28859

Large Displacements and Stability Analysis of Nonlinear Propeller Structures

Robert A. Aiello and Christos C. Chamis
Lewis Research Center
Cleveland, Ohio

Prepared for the
Tenth NASTRAN User's Colloquium
sponsored by NASA/COSMIC
New Orleans, Louisiana, May 13–14, 1982

NASA

ORIGINAL PAGE IS
OF POOR QUALITY

LARGE DISPLACEMENTS AND STABILITY ANALYSIS OF NONLINEAR PROPELLER STRUCTURES

Robert A. Aiello and Christos C. Chamis

National Aeronautics and Space Administration
Lewis Research Center
Cleveland, Ohio 44135

SUMMARY

This paper describes the use of linear rigid formats in COSMIC NASTRAN without DMAP procedures for the analysis of nonlinear propeller structures. Approaches for updating geometry and applying follower forces for incremental loading are demonstrated. Comparisons are made with COSMIC NASTRAN rigid formats and other independant finite element programs. Specifically, the comparisons include results from the four approaches for updating the geometry using RIGID FORMAT 1, RIGID FORMATS 4 and 13, MARC and MSC/NASTRAN. It is shown that "user friendly" updating approaches (without DMAPS) can be used to predict the large displacements and instability of these nonlinear structures. These "user friendly" approaches can be easily implemented by the user and predict conservative results.

E-1229

INTRODUCTION

The potential for high propulsive efficiency in the Mach 0.7 to 0.8 speed range has renewed interest in turboprop propulsion in recent years. Advanced turboprop concepts feature thin, highly swept and twisted propeller blades to achieve high efficiency and low noise at cruise. Deflections due to centrifugal loading, for blades of this type, exhibit a high degree of nonlinearity requiring special analysis techniques not automatically available in COSMIC NASTRAN.

As stated in the NASTRAN Theoretical Manual, "An important limitation of the automatic geometric nonlinear procedures provided with (COSMIC) NASTRAN is in the assumption that the applied loads from which the differential stiffness is derived remain fixed in magnitude and direction during deformation of the structure, and that their points of application move with the structure". This assumption is not valid for swept cantilever type structures like turboprop blades in a centrifugal force field where the direction and magnitude of the force vector is determined by the displaced position of the structure.

Highly swept turboprop blades in a centrifugal force field may experience an abrupt reversal of tip deflection or a large change in tip-chord angle as the rotational speed is increased. These sudden changes in position can severely affect aerodynamic performance and are referred to as instability points in this paper. The objective of this paper is to describe a study conducted on a representative advanced turboprop blade configuration. The selected configuration has a sweep angle of 60° which is at the high end of a range of sweep angles being considered for the advance turboprop concept. The purpose of the study was to investigate high tip displacements, inherent in these designs, using NASTRAN without DMAP alters. The study included the use of RIGID FORMATS 1, 4 and 13. Results obtained from these RIGID FORMATS are compared with each other and with other finite element programs. The mathematical description of the various methods used is summarized in the appendix.

ORIGINAL PAGE IS
OF POOR QUALITY

TURBOPROP GEOMETRY AND FINITE ELEMENT MODEL

The model of the scaled turboprop blade shown in figure 1 is about 10 inches long, has a tip chord of 2 inches, and a maximum chord at the hump of about 3.5 inches. The thickness varies from 1 inch at mid chord at the root to 0.040 inch at mid chord at the tip. The leading edge thickness varies from 0.180 inch at the root to 0.022 inch at the tip. The trailing edge thickness varies from 0.077 inch at the root to 0.016 inch at the tip. The blade has a twist of 33.2°, a sweep angle of 60° and was assumed to be made of titanium. This blade was never built because of predicted high deflections and stresses at operating speeds.

The NASTRAN finite element model is show in figure 2. This model consists of 423 grid points, 744 CTRIA2 elements and 2466 unrestrained degrees of freedom. The model was restrained along the bottom of the shank. The middle node was restrained in all 6 degrees of freedom and the other six nodes were restrained in 5 degrees of freedom with translation allowed in the direction of the spin axis.

RIGID FORMAT 1 (STATIC SOLUTION)

RIGID FORMAT 1 was used to investigate the turboprop geometric nonlinearities in four ways:

Case (1) (RF1-1) Updated Geometry/Angular Speed Difference - A centrifugal force field was applied to the model in increments of 1500 revolutions per minute. Nodal displacements and nodal forces (load vectors generated from the applied speed increment plus the summation of load vectors from previous steps) at each increment were stored in computer disk files. After each step grid locations were updated by adding the nodal displacements to the previous grid points and a new summation of force vectors was created by adding the applied load vectors to the previous summation of load vectors. The new set of grid locations defined the deformed model position for the next increment and the force vectors defined the load required to reach that position. The centrifugal force field applied at each step was equal to the square root of the difference of the new speed squared minus the last speed squared. The mathematical description for this case is summarized in section 1 of the appendix. Seven NASTRAN runs were made from 1500 to 10 500 rpm. Tip rotations and positions were used to identify the onset of instability (fig. 3). For this case the large tip displacement between 4500 rpm and 6000 rpm (fig. 3(b)) was clearly indicative of the onset of structural instability. The change in tip-chord angle for this case (fig. 3(a)) was not as indicative of instability as the change in tip-chord position. The tip displacement also changes directions as the angular speed increases from 4500 rpm to 6000 rpm (figure 3(b)). The tip displacement becomes progressively larger as the angular speed is increased to 9000 rpm and then changes direction again at 10 500 rpm indicating another region of instability. This method is straight forward and easy to apply using NASTRAN RIGID FORMAT 1. The predicted angular speeds causing instability are conservative (pessimistic) and, if accepted, will lead to design modifications to avoid the speeds causing instability.

Case (2) (RF1-2) Updated Geometry/Angular Speed - A centrifugal force field was applied to the model in increments of 1500 rpm. Nodal displacements at each increment were stored in computer disk files. After each step grid locations were updated by adding the nodal displacements to the previous grid

ORIGINAL PAGE IS
OF POOR QUALITY

points. The new set of grid locations defined the deformed model position for the next increment. The total angular speed was applied to this updated position. The mathematical description of this case is summarized in section 2 of the appendix. Seven NASTRAN runs were made from 1500 to 10 500 rpm. Again, tip-chord rotations and positions were used to identify the onset of instability (fig. 4). For this case the onset of instability can be noted from the large tip displacement and change in direction between 4500 rpm and 6000 rpm (fig. 4(b)). Again, the change in tip-chord angle was not as indicative of instability as the change in position. The change in tip-chord position from 9000 rpm to 10 500 rpm is more dramatic than in case (1). This method, also, is straight forward and very easy to apply using NASTRAN RIGID FORMAT 1. The predicted points of instability onset occur at lower rotor speeds than those using the method of case (1). Compared to the other two cases using RIGID FORMAT 1, this case has the following advantages: (a) provides the most pronounced prediction of instability, (b) requires only one computer disk file for storage of displacements, and (c) is straight forward and easiest to apply.

Case (3) (RF1-3) Updated Geometry/Angular Speed/Restraining Forces - A centrifugal force field was applied to the model in increments of 1500 rpm. Nodal displacements and nodal forces (load vectors generated by the applied rotational speed) at each increment were stored in computer disk files. After each step, grid locations were updated by adding the nodal displacements to the previous grid points. The new set of grid locations defined the deformed model position for the next increment. New force vectors were then created from the NASTRAN generated loads resulting from the current applied rotational speed. These force vectors were applied in the opposite sense at the next speed increment and represented blade internal restraining forces (relative equilibrium with the deformed shape). The full rotational speed was applied at the next increment. The mathematical description of this approach is summarized in section 3 of the appendix. Seven NASTRAN runs were made from 1500 to 10 500 rpm. Tip-chord rotations and positions were used to identify the onset of instability (fig. 5). As for the previous two cases, the onset of instability is noted by the large tip displacement between 6000 rpm and 7500 rpm (fig. (5b)). The change in tip-chord angle was not as indicative of instability as the change in position. The point of instability is indicated by the change in tip-chord position from 6000 rpm to 7500 rpm (fig. 5(b)). This approach does not subject the deformed turboprop to the full angular speed at the end of each increment. Therefore, the turboprop deforms the least compared to the previous two cases and, consequently, has the smallest effect on the predictions for the vibration frequencies. Predictions of blade frequencies will be discussed later.

Case (4) (RF1-4) Updated Geometry (Displacement Increment)/Angular Speed Difference - A centrifugal force field was applied to the model in increments of 1500 rpm. Nodal displacements and nodal forces (load vectors generated from the applied speed increment plus applied load vectors from previous step) at each increment were stored in disk files. After each step, grid locations were updated by adding the nodal displacement increments (current minus previous) to the previous grid points and new force vectors were created. The new set of grid locations defined the deformed model position for the next increment and the force vectors defined the load required to reach that position. The centrifugal force field applied at each step was equal to the square root of the difference of the new speed squared minus the last speed squared. The mathematical description for this case is summarized in section 4

ORIGINAL PAGE IS
OF POOR QUALITY

of the appendix. Seven NASTRAN runs were made from 1500 rpm to 10 500 rpm. Tip-chord rotations and positions were used to identify the onset of instability (fig. 6). For this case the jump in chord position from 9000 rpm to 10 500 rpm (fig. 6(b)) is clearly indicative of the onset of structural instability. The change in tip-chord angle for this case (fig. 6(a)) is not at all indicative of instability. It shows possible angle-change leveling-off at higher rotor speeds. The tip-chord also changes direction as the angular speed increases from 3000 rpm to 4500 rpm (fig. 6(b)). The accompanying tip displacements become progressively larger as the angular speed is increased to 9000 rpm and then changes direction again at 10 500 rpm indicating another region of instability. This method is also straight forward and easy to apply using NASTRAN RIGID FORMAT 1. The predicted angular speeds causing instability are higher than case (1) or case (2) and about the same as case (3). This is the only case which predicts a possible leveling-off in tip-chord angle. However, intermediate points are needed to ascertain leveling-off in tip-chord angle with increasing rotor speed.

The nonlinear structural response predicted using RF1-4 is judged to be the most accurate of the various methods examined herein. The accuracy of the method relative to error estimates and relative to experimental data remains to be determined.

RIGID FORMAT 4 (RF4) (NONLINEAR SOLUTION)

As stated in the NASTRAN User's Guide, "RIGID FORMAT 4 is a second order approximation to nonlinear effects of large deflections which computes the differential stiffness matrix by an iterative technique and treats the new matrix as a load correction. The internal loads are thus not linearly related to the applied loads". (See NASTRAN User's Guide). The mathematical description for this case is summarized in section 5 of the appendix.

For each step the load was divided into six increments and the differential stiffness matrix was iterated until the value of the ratio of energy error to total energy was less than 0.001.

The iterative solution for the differential stiffness matrix indicated divergence for speeds above 7500 rpm. For the four load cases, 3000, 4500, 6000, and 7500 rpm, the number of iterations required to meet the convergence criteria was 2, 3, 4, and 7, respectively. The results are plotted in figure 7. The points of instability are easily identified in figure 7(b) where the tip-chord displacement changes direction from 4500 to 6000 rpm. These results are analogous to those for case (1) with the exception that the tip-chord rotation increases less with angular speed up to 7500 rpm.

This method is automatically applied. Its shortcoming is that the new load increment remains fixed in magnitude and direction during deformation of the structure. However, judicious interpretation of the results can provide the instability information needed.

RIGID FORMAT 13 (RF13)

(Normal Modes with Differential Stiffness)

RIGID FORMAT 13 is a one step differential stiffness solution in which the applied loads are assumed to move with their points of application and remain fixed in magnitude and direction. The differential stiffness matrix is computed from the internal element loads resulting from the static solution. RIGID FORMAT 13 combines the differential stiffness with the original stif-

ORIGINAL PAGE IS
OF POOR QUALITY

fness matrix to solve the eigenvalue problem and obtain the normal modes solution. The mathematical description for this case is summarized in section 5 of the appendix.

Results for tip-chord rotation and tip-chord position are shown in figure 8. Though a change in tip-chord displacement occurs between 2500 and 5000 rpm, it is difficult to identify points of instability using this RIGID FORMAT. Note that the tip-chord displacement changes more slowly as the angular speed increases above 5000 rpm. Compared to the methods described previously, RIGID FORMAT 13 predicts (1) tip-chord rotation which is somewhat more severe than RF1-4 and (2) tip-chord position change which is less severe. It appears that RF13 will yield reasonable solutions of the geometry nonlinearities including frequencies with the possible exception of impending structural instabilities.

COMPARISON OF RESULTS

The tip-chord rotation is an important design parameter. It affects the angle of attack which influences the efficiencies, as well as noise and aeroelastic characteristics of the propeller. Predicted tip-chord rotations obtained as described previously are compared with each other and with those predicted by three other methods in figure 9. These three other methods are: (1) ICP-independent contractor program, section 6 of the appendix, (2) MSC/NASTRAN (McNEAL-Schwindler Company NASTRAN - new nonlinear geometry capability) obtained at Ames Research Center, private communication, and (3) MARC obtained at Lewis. It is noted that the MSC/NASTRAN and MARC predicted results were obtained using standard formats. These results are shown here for comparison purposes only and not to imply that this is the best that can be done using MSC/NASTRAN and/or MARC.

The tip-chord rotation curves predicted by RF1-3, RF4 and MARC are almost identical up to angular speeds of 7500 rpm. Those predicted by RF1-4, RF13 and MSC/NASTRAN are about the same and somewhat higher. Those predicted by using the other methods, (RF1-1, RF1-2, and ICP) are, respectively, higher. The results of methods RF1-1 and RF1-2 follow almost identical paths for tip-rotation. However, the method of RF1-2 is much easier to apply. It should be noted that both tip-chord rotations and tip-chord positions are required to properly assess the propeller structural dynamic behavior in view of possible instabilities at higher speeds. In addition, changes in tip-chord rotation affect directly the angle of incidence and, consequently, the efficiency of the turboprop.

VIBRATION FREQUENCIES

The natural frequencies of the blade in the design speed range are important design parameters which affect stability and life prediction. The results of RIGID FORMAT 13 (Normal Modes with Differential Stiffness) applied to the initial grid positions and to the updated grid positions of RF1-2 is shown in figure 10. These curves indicate that the instability point near 9000 rpm and the resulting decrease in natural frequencies would be overlooked if position updating procedures are not applied to RIGID FORMAT 13 analyses. Also, the margins for interference with cyclic disturbances could be misinterpreted and, therefore, adversly influence the turboprop design.

Similar results comparing updated-position frequencies with path-independent frequencies are shown in figure 11. The path-independent frequencies decreases rapidly and at lower rotor speeds leading to overly pessimistic frequency predictions and, perhaps, to major design modifications.

CONCLUSIONS

COSMIC NASTRAN RIGID FORMAT 1 can be used, without recourse to DMAP alters, to predict the nonlinear structural response of swept twisted propellers. RIGID FORMAT 1 with geometry updating using total displacements at each step (RF1-1, 2) can be used to predict the onset of structural instabilities versus rotor speeds. These predictions are comparable to those predicted using methods which are independent of load path and over-estimate the nonlinear structural response. The path-independent method predicts frequencies which are overly pessimistic. RIGID FORMAT 1 with geometry updating using displacement increments (RF 1-4) can be used to predict the overall nonlinear structural response. This approach appears to be the most accurate. RF1-4 predicted results for tip-chord rotation are somewhat below those predicted using RF13 and those predicted by the McNeal-Schwindler Company NASTRAN. RIGID FORMAT 1 with geometry updating using total displacements and negative force (RF1-3) appears to predict nonlinear structural response comparable to those predicted by RIGID FORMAT 4 and MARC. Results predicted by RF1-3 are below those predicted by RF1-4 and underestimate the nonlinear structural response.

ORIGINAL PAGE IS
OF POOR QUALITY

ORIGINAL PAGE IS
OF POOR QUALITY

APPENDIX

MATHEMATICAL DESCRIPTION

The equations describing the mathematics of the several approaches used to obtain nonlinear solutions are summarized in Sections 1 to 6 below. The equations are presented in matrix form. This is a concise description of the many degrees of freedom (DOF) that these equations represent. The notation of the variables used in the equations is as follows: R denotes spatial position (geometry); u denotes deformation from an R spatial position; K denotes stiffness matrix; M denotes mass matrix; Ω denotes rotor speed; Δ denotes increment. The subscript "o" denotes initial position; the subscript F denotes final position; the subscript i denotes the current increment; the subscript j denotes a summation index with limits defined in the given equation. All the variables are referred to the global coordinate system (x, y, z). The equations are summarized in the sequence used. The notation is also summarized in section 7 for convenience.

1. RIGID FORMAT 1, Case (1) (RF1-1) Updated Geometry/Angular Speed Difference - The incremental equations at the ith step for this case are:

$$\{R_{i-1}\} = \{R_{i-2} + u_{i-1}\} \tag{1}$$

$$\Delta\Omega_i^2 = \Omega_i^2 - \Omega_{i-1}^2 \tag{2}$$

$$[K_{i-1}] = [K_{i-2} \quad (R_{i-1})] \tag{3}$$

$$[M_{i-1}] = [M_{i-2} \quad (R_{i-1})] \tag{4}$$

$$\{u_i\} = [K_{i-1}]^{-1} \quad [M_{i-1}]\left\{\Delta\Omega_i^2 \{R_{i-1}\} + \left\{\sum_{j=0}^{i-1} \Delta\Omega_j^2 \{R_j\}\right\}\right\} \tag{5}$$

At $\Delta\Omega_i = \Delta\Omega_F$, $\{R_i\} = \{R_F\}$ (equations (5) and (1)) which is the final deformed spatial position. The total deformation for this case is given by

$$\{U_F\} = \{R_F\} - \{R_o\}$$

The nonlinear geometric effects accumulate progressively in equations (1) to (5) with successive rotor speed increments $\Delta\Omega_i$. Note that the geometry is updated by adding the displacement obtained from equation (5). This accentuates the nonlinear geometric effects and leads to more severe nonlinear response and, therefore, conservative nonlinear structural response.

2. RIGID FORMAT 1, Case (2) (RF1-2) Updated Geometry/Angular Speed - The incremental equations at the ith step for this case are:

$$\{R_{i-1}\} = \{R_{i-2}\} + \{u_{i-1}\} \tag{7}$$

$$[K_{i-1}] = [K_{i-2} \ (R_{i-1})] \tag{8}$$

ORIGINAL PAGE IS
OF POOR QUALITY

$$\left[M_{i-1}\right] = \left[M_{i-2}\ (R_{i-1})\right] \tag{9}$$

$$\{u_i\} = \Omega_i^2 \left[K_{i-1}\right]^{-1} \left[M_{i-1}\right]\left\{R_{i-1}\right\} \tag{10}$$

The final deformed position $\{R_F\}$ is obtained from equations (10) and (7) at $\Omega_i = \Omega_F$. The total deformation is obtained from $\{R_F\} - \{R_O\}$. The nonlinear geometric effects accumulate faster for this case than for RIGID FORMAT 1, Case (1) as can be readily observed by comparing equations (5) and (10). RIGID FORMAT 1, Case (2) will predict more conservative nonlinear structural response than RIGID FORMAT 1 Case (1). However, RIGID FORMAT 1, Case (2) is much easier to implement and will indicate possible unstable spatial positions at lower rotor speeds.

3. RIGID FORMAT 1, Case (3) (RF1-3) Updated Geometry/Angular Speed/Restraining Forces - The incremental equations at the ith step for this case are:

$$\left\{R_{i-1}\right\} = \left\{R_{i-2}\right\} + \left\{u_{i-1}\right\} \tag{11}$$

$$\Omega_i^2 = (\Omega_{i-1} + \Delta\Omega)^2 \tag{12}$$

$$\left[K_{i-1}\right] = \left[K_{i-1}\ (R_{i-1})\right] \tag{13}$$

$$\left[M_{i-1}\right] = \left[M_{i-1}\ (R_{i-1})\right] \tag{14}$$

$$\{u_i\} = \left[K_{i-1}\right]^{-1} \left[M_{i-1}\right] \left\{\Omega_i^2 \left\{R_{i-1}\right\} - \left\{\sum_{j=0}^{i-1} \Delta\Omega_j^2 \left\{R_j\right\}\right\}\right\} \tag{15}$$

The final deformed position is obtained from equations (15) and (11) at $\Omega_i = \Omega_F$. The total deformation $\{U_F\} = \{R_F\} - \{R_O\}$. This case differs from the previous two cases in the way the current displacement $\{U_i\}$ is calculated in equation (15). The full centrifugal force field is not applied at the ith step. The first term in the braces in equation (15) is the full rotor speed at that step (Ω) while the second, which is subtracted from the first, represents the cumulative centrifugal force (Ω_{i-1}). This approach will (1) underpredict the geometric nonlinear effects on structural response, (2) predict higher rotational speeds for impending instabilities and, as a consequence, will be nonconservative. Implementation of this case is comparable to RF1-1.

4. RIGID FORMAT 1 Case (4) (RF1-4) Updated Geometry (Displacement Increment)/Angular Speed Difference. The governing equations at the ith angular speed increment (using the notation defined previously) are given by:

$$\left\{R_{i-1}\right\} = \left\{R_o + \sum_{j=1}^{i-1} \Delta u_j\right\} \tag{16}$$

$$\Delta\Omega_i^2 = \Omega_i^2 - \Omega_{i-1}^2 \tag{17}$$

ORIGINAL PAGE IS
OF POOR QUALITY

$$\left[K_{i-1}\right] = \left[K_o \left(R_o + \sum_{j=1}^{i-1} \Delta u_j\right)\right] \tag{18}$$

$$\left[M_{i-1}\right] = \left[M_o \left(R_o + \sum_{j=1}^{i-1} \Delta u_j\right)\right] \tag{19}$$

$$\{u_i\} = \left[K_{i-1}\right]^{-1} \left[M_{i-1}\right] \left\{\Delta\Omega_i^2 \left\{R_{i-1}\right\} + \left\{\sum_{j=0}^{i-1} \Delta\Omega_j^2 \left\{R_j\right\}_{R_{i-1}}\right\}\right\} \tag{20}$$

$$\{u_i\} = \left\{\sum_{j=1}^{i} \Delta u_j\right\} \tag{21}$$

At $\Delta\Omega_i = \Delta\Omega_F$, $\{U_F\}$ is obtained from equation (20). Subsequently the total deformation is obtained from equation (21) and the final deformed spatial position is obtained from equation (16). Note in equations (16) to (20) that the nonlinear geometric effects enter the equations progressively with each successive rotor speed increment $\Delta\Omega_i$. Note, also, that the total centrifugal force field is used at each R_{i-1} position (equation (20)) increment plus cumulative, as compared to RIGID FORMAT 1, Case (3) (equation (15)) where only the incremental centrifugal field is applied.

5. RIGID FORMATS 4 (RF4) and 13 (RF13) Standard NASTRAN FORMATS - The differential stiffness is used in the solution for both of these formats. Using the previous notation, the governing equation for the differential stiffness is (See the NASTRAN Theoretical Manual)

$$\{u_i\} = \left[K_o + K_d\,(u_o)\right]^{-1} \left\{\Omega_F^2 \left[M_o\right]\left\{R_o\right\} + \left[K_d\,(u_o - u_{i-1})\right] \left\{u_{i-1}\right\}\right\} \tag{22}$$

where K_d is the differential stiffness matrix and $\{U_o\}$ is the initial incremental displacement used to form $[K_d]$. It can be seen in equation (22) that the stiffness matrix $[K] = [K_o + K_d\,(U_o)]$ is formed using initial position variables and that Ω_F is applied to the initial position. As a result, the intermediate spatial positions and, therefore, the progressive nonlinear geometric effects are not represented in either $[K]$ or Ω. Consequently, both RIGID FORMAT 4 and RIGID FORMAT 13 will underpredict the nonlinear geometric effects on structural response. These formats will predict higher rotor speeds for impending structural instabilities. Solutions obtained by using either of these FORMATS will be more unconservative than those obtained by using RIGID FORMAT 1, Case (3).

6. Nonlinear Geometric Solutions Independent of Load Path - The total deformation for his approach is given by

$$\{u_F\} = \left[\left[K_o\right] - \Omega_o^2 \left[M_o\right]\right]^{-1} \left\{\Omega_F^2 \left[M_o\right]\left\{R_o\right\}\right\} \tag{23}$$

Equation (23) will predict infinite $\{U_F\}$ if

$$\left[\left[K_o\right] - \Omega_o^2 \left[M_o\right]\right] = 0 \tag{24}$$

Equation (24) has the form of an eigenvalue problem and, therefore, will cause equation (23) to predict infinite displacements when

$$\Omega_o^2 = \omega^2 \tag{25}$$

or when the rotor speed (Ω) equals any of the natural frequencies (ω) of the structure. Equation (23) will overpredict the nonlinear geometric effects on structural response as well as impending structural instabilities. Consequently, the results will be overly pessimistic.

7. Summary of the Notation used in this Appendix

$[K]$	global stiffness matrix
$[M]$	global mass matrix
$\{R\}$	spatial position (structure geometry) vector
$\{U\}$	global displacement vector
x,y,z	global coordinates
Δ	increment
Ω	rotor speed
ω	natural frequency

Subscripts

F	final
d	differential
i	increment (solution step) index
j	summation index
o	initial

ORIGINAL PAGE IS
OF POOR QUALITY

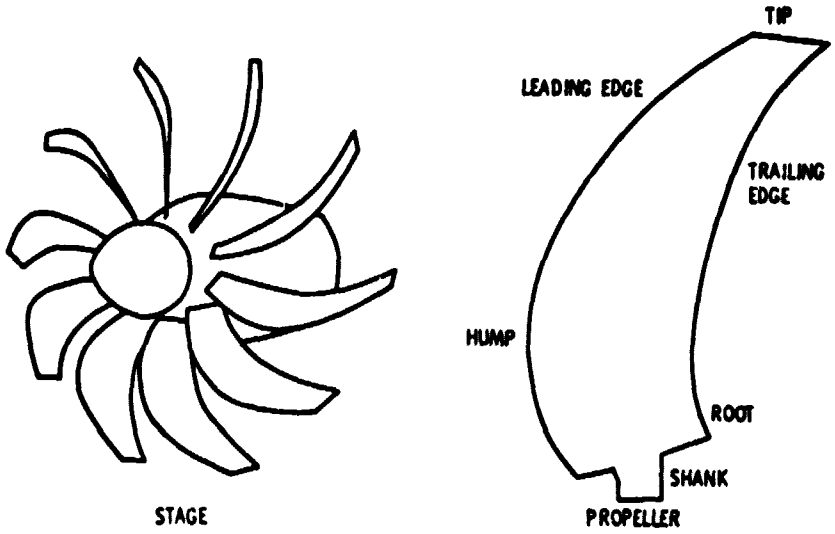

Figure 1. - Turboprop stage and propeller.

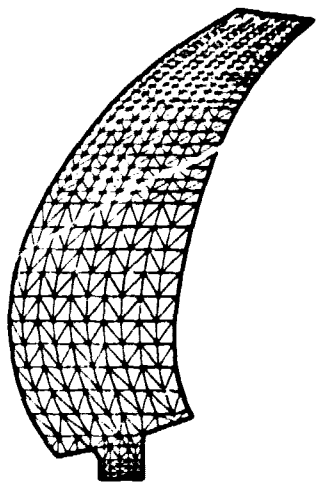

Figure 2. - Turboprop propeller finite element model (423 grid points, 744 elements).

ORIGINAL PAGE IS
OF POOR QUALITY

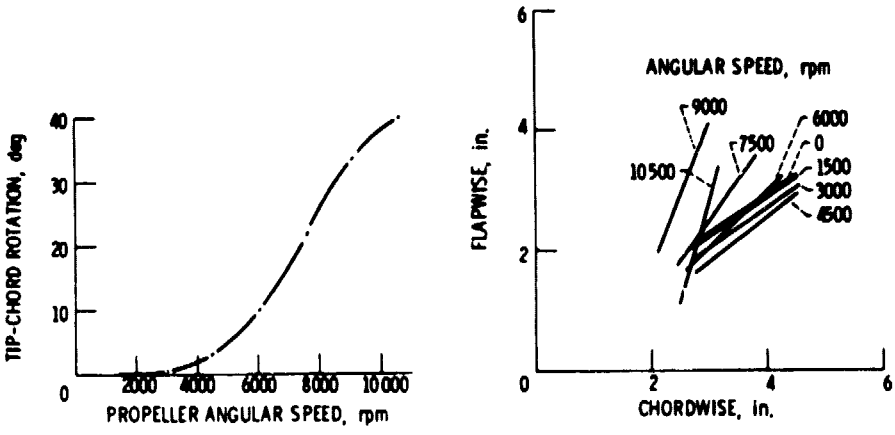

(a) Tip-chord rotation. (b) Tip-chord position.

Figure 3. - Rigid format 1, case (1) - updated geometry and forces/angular speed difference results.

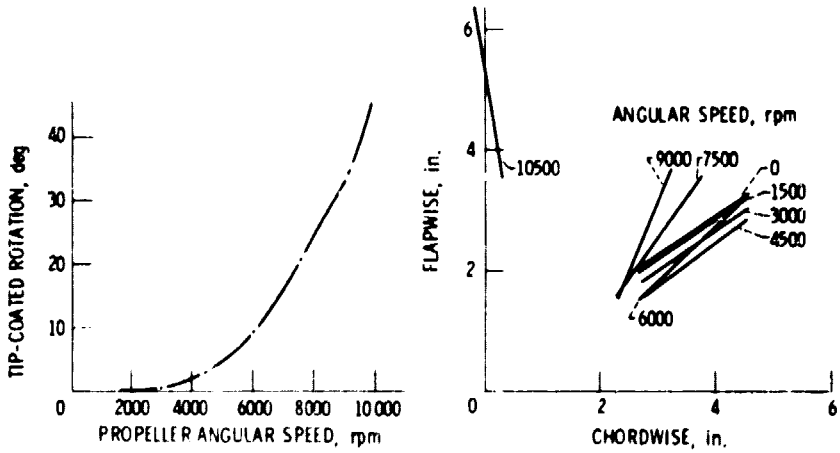

(a) Tip-chord rotation. (b) Tip-chord position.

Figure 4. - Rigid format 1, case (2) - updated geometry/angular speed results.

ORIGINAL PAGE IS
OF POOR QUALITY

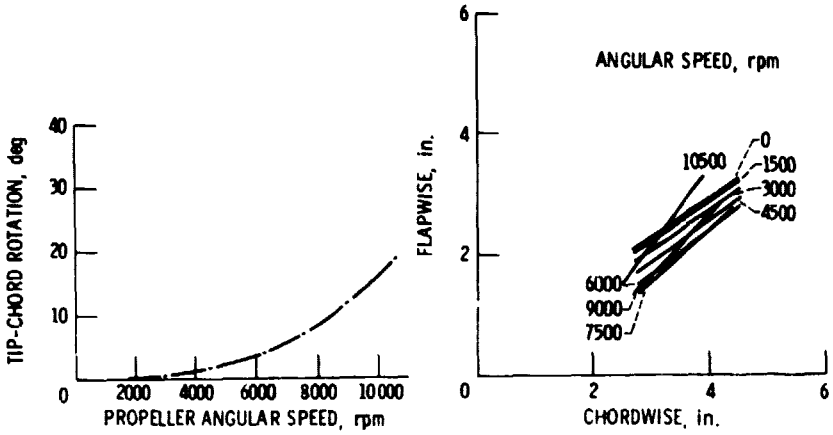

(a) Tip chord rotation. (b) Tip-chord position.

Figure 5. - Rigid format 1, case (3) - updated geometry/angular speed/restraining force results.

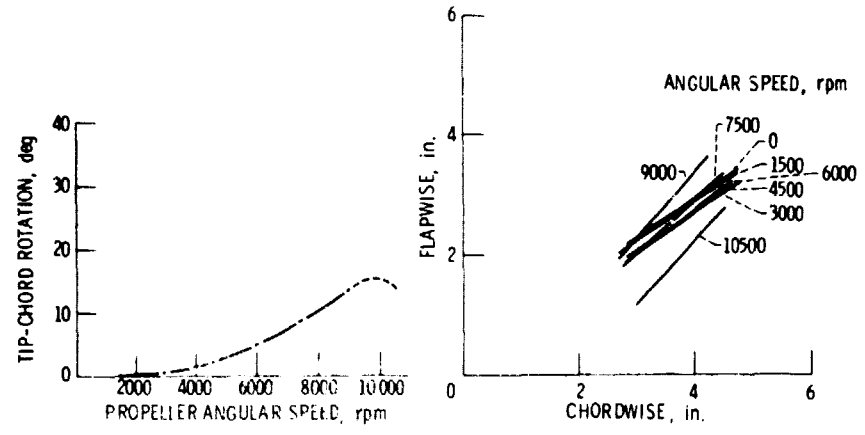

(a) Tip-chord rotation. (b) Tip-chord position.

Figure 6. - Rigid format 1, case (4) - updated geometry displacement increment and forces/angular speed difference results.

ORIGINAL PAGE IS
OF POOR QUALITY

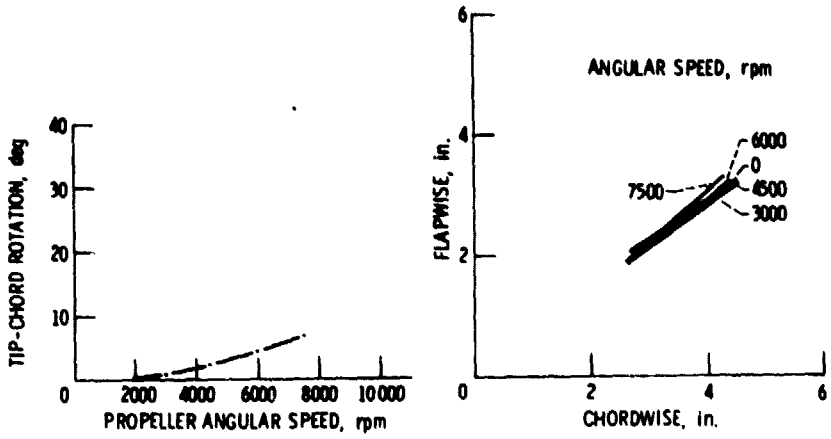

(a) Tip-chord rotation. (b) Tip-chord position.

Figure 7. - Rigid format 4 solution results.

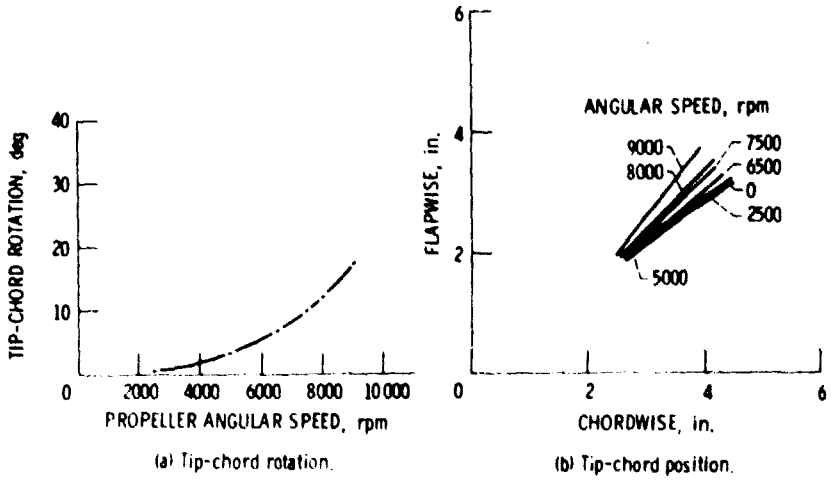

(a) Tip-chord rotation. (b) Tip-chord position.

Figure 8. - Rigid format 13 solution results.

ORIGINAL PAGE IS
OF POOR QUALITY

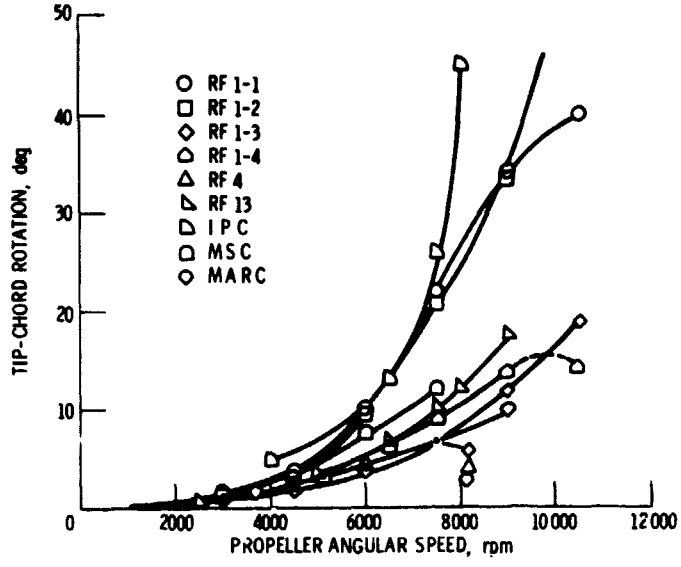

Figure 9. - Comparisons of predicted tip-chord rotation using various methods.

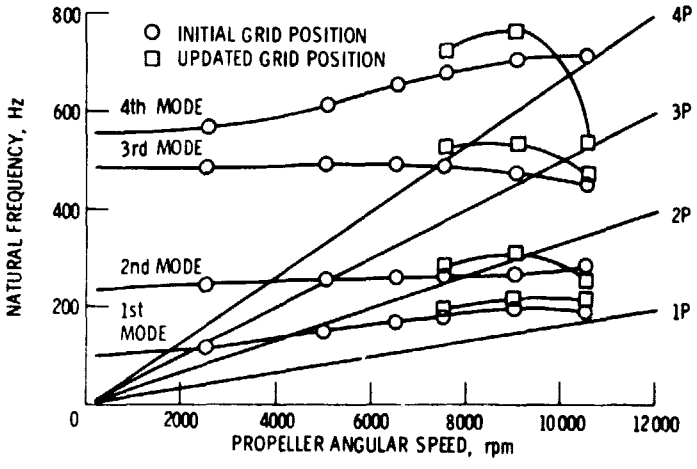

Figure 10. - Campbell diagram showing comparisons of predicted natural frequencies.

ORIGINAL PAGE IS
OF POOR QUALITY

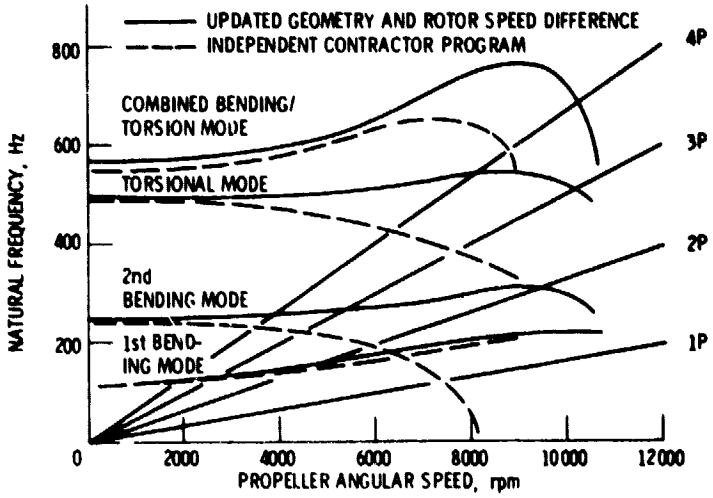

Figure 11. - Campbell diagram showing comparisons of predicted natural frequencies.